Modeling Slope Instability as Shear Rupture Propagation in a Saturated Porous Medium

Final submission, 14 April 2009, for publication in Proceedings,
4th International Symposium on Submarine Mass Movements and Their Consequences,
Austin, TX, 8-11 November 2009

Modeling slope instability as shear rupture propagation in a saturated porous medium

Robert C. Viesca[1] and James R. Rice[1,2]
[1]School of Engineering and Applied Sciences, [2]Department of Earth and Planetary Sciences, Harvard University, 29 Oxford St., Cambridge, MA 02138

Abstract

When a region of intense shear in a slope is much thinner than other relevant geometric lengths, this shear failure may be approximated as localized slip like in faulting, with strength determined by frictional properties of the sediment and effective stress normal to the failure surface. Peak and residual frictional strengths of submarine sediments indicate critical slope angles well above those of most submarine slopes—in contradiction to abundant failures. Because deformation of sediments is governed by effective stress, processes affecting pore pressures are a means of strength reduction. However, common methods of examining slope stability neglect dynamically variable pore pressure during failure. We examine elastic-plastic models of the capped Drucker-Prager type and derive approximate equations governing pore pressure about a slip surface when the adjacent material may deform plastically. In the process we identify an elastic-plastic hydraulic diffusivity with an evolving permeability and plastic storage term analogous to the elastic term of traditional poroelasticity. We also examine their application to a dynamically propagating subsurface rupture and find indications of downslope directivity.

Keywords: Landslide, slope stability, slip surface, friction, pore pressure, storage, diffusivity, poroelasticity, plasticity, dynamic rupture, finite element

1. Introduction

How sediments deform and pore fluid flows during the shearing process has not been precisely determined for the variety of styles of landslides. While some failures may occur at a stratigraphic discontinuity, others may occur within the sediment column. When failure is within the sediment, to what extent that failure is localized is uncertain. Not knowing when and where failure may start hampers field observations of failure initiation and progression. However, a failure location and time can be constrained by artificially creating failure conditions. For example, Cooper et al. (1998) induced slump failure in a naturally deposited clay slope by artificially elevating pore pressures. Excavation revealed an O(mm) thick intense shear zone within an O(cm) thick disturbed region.

Observations of local deformation and apparent progressive failure (Bjerrum 1967, Bishop 1971) inspired treating the shear zone as a slipping fracture and examining criteria for unstable rupture propagation—i.e., criteria for rupture to continue propagation without further loading, presumably the inception of complete slope failure. Palmer and Rice (1973) examined the propagation of rupture from the base of a cut within an overconsolidated clay slope and estimated the rupture length required to initiate unstable growth by gravitational loading. Puzrin and Germanovich (2004, 2005) similarly examined the case of a rupture paralleling the slope surface with the intention of extending the analysis of Palmer and Rice to the failure of slopes composed of normally consolidated clay or incohesive soil. With experimental observations of shear bands in such soils in mind, they postulate that slope failure in these soils would ultimately occur in local deformation-weakening shear zones similar to the failure of overconsolidated clays. Such an analysis lends itself towards examining effective stress controls on slope stability. This is an appealing approach for studying failure in the submarine environment, where slopes are often too shallow for

Published in *Submarine Mass Movements and Their Consequences*, eds. D. C. Mosher, R.C. Shipp, L. Moscardelli, J. D. Chaytor, C. D. P. Baxter, H. J. Lee, and R. Urgeles, Advances in Natural and Technological Hazards Research, Vol. 28, Springer-Verlag New York, pp. 215-223, 2010.

failure to be explained by infinite slope or limit equilibrium analyses. In this environment, processes affecting pore pressure such as local fluid flux (Dugan and Flemings 2000) or methane hydrate dissociation (Xu and Germanovich 2006) have been proposed as mechanisms for initiating failure. The works of Palmer and Rice, and Puzrin and Germanovich, considered the shear strength on the surface to degrade with the amount of slip, assumed that the length of the rupture was much greater than its depth and that the stress-strain relationship of the overlying sediments was linearly elastic until passive or active failure.

The role of fluid in rupture initiation, propagation, and runout is often central in landslide processes. In the experiment of Cooper et al. (1998), decreases in measured pore pressure during early-stage slope movement indicate a stabilizing dilative suction preceding total slope failure. Subaerial flume studies of densely or loosely packed sandy sediment also show a tendency for dilatant stabilization in the case of dense sediments and transition to debris flow when loosely packed (Iverson et al. 2000). Monitoring shearing rates and pore pressures in a ring shear apparatus, Moore and Iverson (2002) observe the diffusive nature of such stabilization in relatively coarse- and fine-grained sediments.

The question remains how to appropriately determine the pore pressure within a finite thickness shear zone approximated by a sliding surface. Specifically, contributions from processes within the shear zone may be lumped into the surface behavior in addition to contributions from material deformation beyond the shear zone. When concerned with slip-surface pore pressures, current modeling of dynamic rupture propagation has included inelastic porosity changes as either a slip-proportional porosity change (Rice 1980, Suzuki and Yamashita 2008) or a transition to a rate-dependent steady-state porosity (Segall and Rice 1995, Bizzarri and Cocco 2006). Other work has examined slip propagating quasi-statically or dynamically in a saturated poroelastic or poro-elastic-plastic media, but neglected the effect of pore pressure changes on the fault on shear strength (de Borst et al. 2006, Réthore et al. 2007, Viesca et al. 2008).

In addition to the inelastic processes occurring within the surface-approximated shear zone are those about the rupture tip. The rupture criterion set by the surface weakening behavior eliminates stress singularities, however there remain significant stress concentrations. It is well known in dynamic shear rupture that in such cases regions of inelastic deformation grow, with propagation, to dimensions significant in comparison to rupture length (e.g., Templeton and Rice 2008) and one can expect such regions of failure around the rupture tip in the quasi-static limit. In the following we propose a model in which pore pressure on the slip-surface is determined by the poro-elastic-plastic deformation and consequent fluid flux surrounding the slip surface. This parallels efforts to discretize the poro-mechanical deformation of a finite-thickness shear zone (e.g., White and Borja 2008).

2. Determining pore pressures at a sliding interface with plastically deforming surroundings

The saturated porous material deforms elastically until a yield condition is met. The condition is given by a function F of the effective stress (positive in tension) $\bar{\boldsymbol{\sigma}} = \boldsymbol{\sigma} + p\mathbf{I}$, where $\boldsymbol{\sigma}$ is the total stress tensor and p is the pore fluid pressure, and potentially a function of other state variables, such as the void ratio or a magnitude of plastic strain. $F(\bar{\boldsymbol{\sigma}}) = 0$ is the yield condition. Here the yield function is expressed in terms of the stress invariants $\mathrm{tr}\,\bar{\boldsymbol{\sigma}}/3$ and $\bar{\tau} = \sqrt{\mathbf{s}:\mathbf{s}/2}$ where $\mathbf{s} = \boldsymbol{\sigma} - \mathrm{tr}\,\boldsymbol{\sigma}\mathbf{I}/3$ is the deviatoric part of the stress tensor. Figure 1 is an illustration of such a function where $\mu = \partial F / \partial(\mathrm{tr}\,\bar{\boldsymbol{\sigma}}/3)$ is the

local measure of the pressure-dependence of the criterion and b is the cohesive strength. During continued plastic deformation, the stress state must satisfy either $\partial F / \partial \bar{\boldsymbol{\sigma}} : d\bar{\boldsymbol{\sigma}} = 0$ to move along the yield surface or $\partial F / \partial \bar{\boldsymbol{\sigma}} : d\bar{\boldsymbol{\sigma}} > 0$ to follow the outward evolution of the yield surface. Here, we allow the yield surface to evolve with plastic strain and define the hardening modulus, $\partial F / \partial \bar{\boldsymbol{\sigma}} : d\bar{\boldsymbol{\sigma}} = h d\gamma^{pl}$

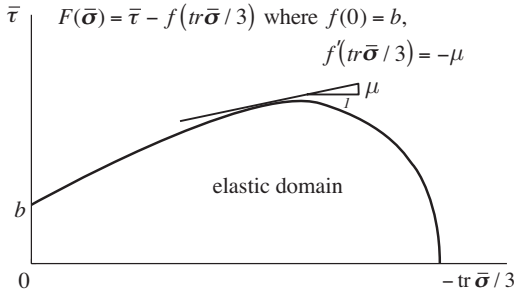

Figure 1: Illustration of pressure-dependent yield criterion F.

where $d\gamma^{pl} = \sqrt{2 d\mathbf{e}^{pl} : d\mathbf{e}^{pl}}$, and $d\mathbf{e}^{pl} = d\boldsymbol{\varepsilon}^{pl} - (\operatorname{tr} d\boldsymbol{\varepsilon}^{pl})\mathbf{I}/3$. A second potential $H(\bar{\boldsymbol{\sigma}})$ (here, of similar form to F) indicates the direction of plastic strain increments: $d\boldsymbol{\varepsilon}^{pl} = d\gamma^{pl} \partial H / \partial \bar{\boldsymbol{\sigma}}$. From the potentials F and H, we define the second order tensors

$$\mathbf{Q} = \frac{\partial F}{\partial \bar{\boldsymbol{\sigma}}} = \frac{\mathbf{s}}{2\bar{\tau}} + \frac{\mu}{3}\mathbf{I} \qquad \mathbf{P} = \frac{\partial H}{\partial \bar{\boldsymbol{\sigma}}} = \frac{\mathbf{s}}{2\bar{\tau}} + \frac{\beta}{3}\mathbf{I} \qquad \text{(X.0)}$$

where $\beta = \partial H / \partial(\operatorname{tr}\bar{\boldsymbol{\sigma}} / 3)$ is the ratio $\operatorname{tr} d\boldsymbol{\varepsilon}^{pl} / d\gamma^{pl}$. More explicitly, we decompose the total strain increment into elastic and plastic components $d\boldsymbol{\varepsilon} = d\boldsymbol{\varepsilon}^{el} + d\boldsymbol{\varepsilon}^{pl}$, and the plastic strain increments may be written as $d\boldsymbol{\varepsilon}^{pl} = \mathbf{P}(\mathbf{Q} : d\bar{\boldsymbol{\sigma}}) / h$. Increments in the Biot effective stress $d\boldsymbol{\sigma} + \alpha dp\mathbf{I}$ are determined by increments in elastic strain, $d(\boldsymbol{\sigma} + \alpha p\mathbf{I}) = \mathbf{L} : (d\boldsymbol{\varepsilon} - d\boldsymbol{\varepsilon}^{pl})$, where $\mathbf{L}$ is the elastic stiffness tensor described below.

The increments of elastic-plastic total stress and pore fluid mass m (with fluid density ρ) may be written in terms of those of strain and pore pressure (e.g., Rudnicki 2001)

$$d\boldsymbol{\sigma} = \left(\mathbf{L} - \frac{(\mathbf{L}:\mathbf{P})(\mathbf{Q}:\mathbf{L})}{h + \mathbf{Q}:\mathbf{L}:\mathbf{P}} \right) : d\boldsymbol{\varepsilon} - \left(\alpha\mathbf{I} + \frac{(1-\alpha)\operatorname{tr}\mathbf{Q}(\mathbf{P}:\mathbf{L})}{h + \mathbf{Q}:\mathbf{L}:\mathbf{P}} \right) dp \qquad \text{(X.1)}$$

$$\frac{dm}{\rho} = \left(\frac{\alpha(1-\alpha B)}{KB} + \frac{(1-\alpha)^2 \operatorname{tr}\mathbf{P} \operatorname{tr}\mathbf{Q}}{h + \mathbf{Q}:\mathbf{L}:\mathbf{P}} \right) dp + \left(\alpha\mathbf{I} + \frac{(1-\alpha)\operatorname{tr}\mathbf{P}(\mathbf{P}:\mathbf{L})}{h + \mathbf{Q}:\mathbf{L}:\mathbf{P}} \right) : d\boldsymbol{\varepsilon} \qquad \text{(X.2)}$$

In all bracketed terms preceding dp and $d\boldsymbol{\varepsilon}$, the first term corresponds to the elastic response and the second to the contribution of plastic deformation. The elastic coefficients are $\mathbf{L}$, the fourth-order linear-elastic stiffness tensor (i.e., for isotropic elasticity and a second-order symmetric tensor $\mathbf{A}$, $\mathbf{L} : \mathbf{A} = \mathbf{A} : \mathbf{L} = K\mathbf{I} \operatorname{tr}\mathbf{A} + 2G \operatorname{dev}\mathbf{A}$, where K and G are the bulk and shear moduli), and B, the poroelastic Skempton coefficient.

Taking the boundary-layer approximation and considering gradients parallel to the slip surface to be much smaller than the normal gradients, the conservation of fluid mass near the surface requires $\partial q / \partial y = -\partial m / \partial t$, where q is the pore fluid mass flux given by Darcy's law $q = -(\rho k / \eta)\partial p / \partial y$, k being the permeability and η the permeating fluid viscosity. Combining fluid conservation and Darcy's law

$$\frac{\rho k}{\eta} \frac{\partial^2 p}{\partial y^2} = \frac{\partial m}{\partial t} \qquad \text{(X.3)}$$

In calculating the rate of the fluid mass, we consider the region around the slip surface as consisting of material that may differ in mechanical behavior (e.g., elastic stiffness, dilation, and internal friction) from the typical response of the sediment further away from the slip surface (i.e., a disturbed region about the slip surface). The adjoining materials are

coupled by the continuity of certain components of stress σ_c ($\sigma_{yx}, \sigma_{yy}, \sigma_{yz}$) and strain ε_c ($\varepsilon_{xx}, \varepsilon_{zz}, \varepsilon_{xz}$), the remaining free components of stress and strain are designated as σ_f ($\sigma_{xx}, \sigma_{zz}, \sigma_{xz}$) and ε_f ($\varepsilon_{xy}, \varepsilon_{yy}, \varepsilon_{yz}$). With this in mind, we rearrange (X.1) and (X.2) into vector and matrix notation where

$$\{d\sigma\} = d\begin{Bmatrix}\{\sigma_c\}\\ \{\sigma_f\}\end{Bmatrix} \text{ and } \{d\varepsilon\} = d\begin{Bmatrix}\{\varepsilon_c\}\\ \{\varepsilon_f\}\end{Bmatrix} \tag{X.4}$$

such that

$$\begin{aligned}\{d\sigma_c\} &= [N_{11}]\{d\epsilon_c\} + [N_{12}]\{d\varepsilon_f\} + \{U_1\}dp\\ \{d\sigma_f\} &= [N_{21}]\{d\epsilon_c\} + [N_{22}]\{d\varepsilon_f\} + \{U_2\}dp\\ \frac{dm}{\rho} &= Cdp + \{M_1\}^T\{d\varepsilon_c\} + \{M_2\}^T\{d\varepsilon_f\}\end{aligned} \tag{X.5–7}$$

[N], {M}, {U}, C are the matrix, vector, and scalar coefficients whose components are determined by the constitutive relationships (X.1) and (X.2). For example, in *xy* plane strain

$$\{U_1\}^T = \left\{ -\left(\alpha + \frac{(1-\alpha)\mu\left(Gs_{xy}/\bar{\tau}\right)}{h+G+\mu\beta K}\right) \quad -\frac{(1-\alpha)\mu\left(\beta K + Gs_{yy}/\bar{\tau}\right)}{h+G+\mu\beta K} \right\} \tag{X.8}$$

Expressing $\{d\varepsilon_f\}$ in terms of $\{d\varepsilon_c\}$, $\{d\sigma_c\}$, and dp, (X.9) reduces to

$$\frac{dm}{\rho} = \beta_{stor}dp + \{R\}^T\{d\varepsilon_c\} + \{S\}^T\{d\sigma_c\} \tag{X.9}$$

where $\beta_{stor} = C - \{M_2\}^T[N_{12}]^{-1}\{U_1\}$, $\{R\}^T = \{M_1\}^T - \{M_2\}^T[N_{12}]^{-1}[N_{11}]$, and $\{S\}^T = \{M_2\}^T[N_{12}]^{-1}$.

During elastic response, β_{stor} is the poroelastic storage coefficient under one-dimensional consolidation ($d\varepsilon_{xx} = d\varepsilon_{zz} = 0$), $\beta_{stor} = \beta_{stor}^{el} = \left[\left(K_u + 4G/3\right)/\left(K + 4G/3\right)\right]\alpha / BK_u$, where $K_u = K/(1-\alpha B)$ is the undrained bulk modulus. During plastic deformation, $\beta_{stor} = \beta_{stor}^{pl}$ is a plastic storage coefficient for one-dimensional straining that reflects a compressibility increase with yielding. We see from (X.1–2b) that during plastic loading the components depend not only on the elastic-plastic material parameters, but also on the scaled deviatoric stress components. For plane conditions ($s_{xz} = s_{yz} = 0$) and $s_{zz} = 0$ ($s_{xx} = -s_{yy}$), $\bar{\tau} = s_{xx}^2 + s_{xy}^2$. Deviatoric stress states can then be characterized

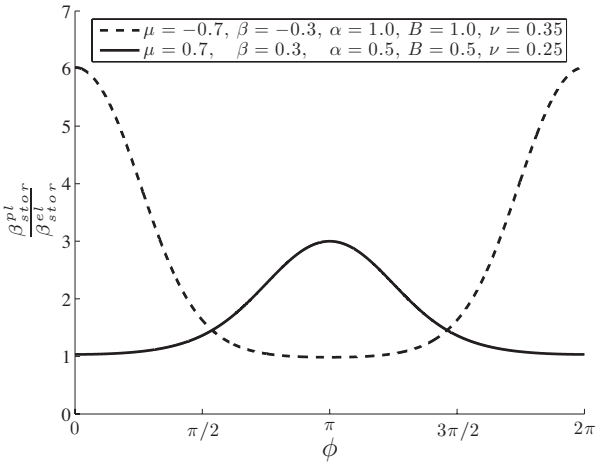

Figure 2: Plot of factor of increase in storage coefficients (compressibilities) with onset of ideally plastic ($h = 0$) yielding for compacting sediment (dashed) and dilating rock (solid) over a range of stress states for which $s_{zz} = 0$, $s_{xy}/\bar{\tau} = \sin\phi$, and $s_{xx}/\bar{\tau} = -s_{yy}/\bar{\tau} = \cos\phi$.

by an angle ϕ ($s_{xx} = -s_{yy} = \bar{\tau}\cos\phi$, $s_{xy} = \bar{\tau}\sin\phi$), and the expression for β_{stor}^{pl} is reduced to a dependence on ϕ and material parameters. Considering poro-elastic-plastic parameters representative of a low-porosity rock (e.g., Rudnicki and Rice 1975, Rice and Cleary 1976), for which yielding will occur on the dilative side of the yield surface ($\mu > \beta > 0$) for most stress states, the storage may increase threefold (Figure 2). For sediment with pore fluid and component particles much stiffer than the matrix as a whole (i.e., $\alpha = B = 1$) yielding on the compacting side of the yield surface (right side of Figure 1), we find the plastic storage may increase sixfold.

Setting $dm = 0$ in (X.9) defines the undrained pore pressure increment dp_u adjacent to the slip surface. (X.9) can be rewritten $dm/\rho = \beta_{stor} d(p - p_u)$ and (X.5) reduces to

$$\frac{k}{\beta_{stor}\eta_f}\frac{\partial^2 p}{\partial y^2} = \frac{\partial}{\partial t}(p - p_u) \qquad \text{(X.10)}$$

In the poroelastic case, $dp_u = -[2G(d\epsilon_{xx} + d\epsilon_{zz}) + d\sigma_{yy}]B(1+\nu_u)/3(1-\nu_u)$ where the increments in these stresses and strains can be considered explicitly as functions of time (i.e, within the boundary layer of the disturbed region there is no y-dependence of these increments, which are determined by the coupling to the bulk). Consequently, (X.10) can be rewritten such that the pressure difference from the undrained value satisfies

$$\alpha_{hy}\frac{\partial^2}{\partial y^2}(p - p_u) = \frac{\partial}{\partial t}(p - p_u) \qquad \text{(X.11)}$$

where $k/\beta_{stor}^{el}\eta$ is the hydraulic diffusivity α_{hy}. Keeping fluid flux and pore pressures continuous across the slip surface, the pore pressure across the surface can be determined. Rudnicki and Rice (2006) found an analytical solution for the surface pressure based on the undrained pressures and hydraulic properties above (+) and below (–) the surface

$$dp_s = \zeta^+ dp_u^+ + \zeta^- dp_u^- \qquad \zeta^{\pm} = \frac{\left(\sqrt{k\beta_{stor}^{el}}\right)^{\pm}}{\left(\sqrt{k\beta_{stor}^{el}}\right)^{-} + \left(\sqrt{k\beta_{stor}^{el}}\right)^{+}} \qquad \text{(X.12)}$$

In mode-II shear rupture, one side of the ruptured surface undergoes compression (pressurization) and the other extension (suction). The influence of each side on the surface pressure is determined by the hydraulic property contrast in the weighting (X.12). Dunham and Rice (2008) modeled plane-strain bilateral dynamic ruptures with the above solution and found preferences in rupture direction for hydraulic property contrasts thought to be typical of faults.

However, this solution breaks down once the material begins to yield. Most notable is the expected change in permeability with plastic deformation. For some fine-grained sediment, moderate changes in void ratio (0.1–0.2) can produce 1–2 order of magnitude changes in permeability (Lambe and Whitman 1969). For low-porosity rock, monitoring of permeability and inelastic deformation during triaxial tests of intact granodiorite and granite shows 1–2 orders of magnitude increases in permeability for axial inelastic strains of the order 0.1% (e.g., Mitchell and Faulkner 2008). This effect on its own introduces a time-dependence to the hydraulic diffusivity not accounted for in (X.12). More subtle effects may result when considering changes in pore pressure across the slip surface. One such effect may be that these changes result in some slip surface adjacent material moving away from yield (i.e., some material within each boundary layer deforms plastically, and some

elastically). An even more subtle effect with plastic deformation is the effect that the changes in pressure have in determining deviatoric stress components. The poroelastic expression for dp_u could explicitly be written as a function of time (i.e., no y-dependence) and as a result the diffusion equation could be reached. This is generally not the case during plastic deformation. In the expression for dp_u there is a dependence on the components of $\mathbf{s}/\bar{\tau}$, which will vary with the changes in pressure across the slip surface introducing a y-dependence of dp_u.

Solving for the pore pressure at the slip surface requires addressing these deviations from the poroelastic diffusion equation. However, such a solution is nontrivial and we seek to make it more tractable. One such simplification is to assume that permeability changes are uniform within each boundary layer. Consistent with this is to neglect switching between elastic or plastic deformation within each boundary layer (i.e., the boundary layer undergoes either elastic or plastic deformation). Lastly, we neglect surface-normal variations in $\mathbf{s}/\bar{\tau}$ such that dp_u and β_{stor}^{pl} are determined by the coupled stress components (i.e., depend explicitly on time alone). With these assumptions, (X.10) becomes

$$\alpha_{hy}^{pl}(t)\frac{\partial^2}{\partial y^2}\left(p-p_u\right)=\frac{\partial}{\partial t}\left(p-p_u\right) \qquad \text{(X.13)}$$

where $\alpha_{hy}^{pl}(t)=k(t)/\beta_{stor}^{pl}(t)\eta$ is an elastic-plastic diffusivity.

3. Finite element model of a dynamic subsurface rupture

We use the finite element method (with ABAQUS/Explicit) to examine the dynamic propagation of a subsurface shear rupture. Dynamic rupture propagation (i.e., where inertial effects are in the equation of motion and shear rupture speeds are of the order of the shear wave speed c_s), while not typically considered for slope stability, is actively investigated in the earthquake rupture community. We use such an approach here to gain insights into influential processes at the rupture front. The treatment of the model domain is similar to that described in Templeton and Rice (2008) and Viesca et al. (2008), who examined rupture in an unbounded medium. 4-noded plane-strain, reduced-integration elements compose the bulk and a predefined split-node interface represents a likely failure plane. The surface corresponds to the slope surface, and absorbing elements ("infinite elements" in ABAQUS) are applied downslope and upslope, and at a slope-perpendicular depth to simulate infinite slope conditions and minimize reflections other than from the free surface.

The shear strength τ at the slip surface is effective-stress dependent, $\tau=f\bar{\sigma}=f(\sigma-p_s)$ where the scalar total and effective surface-normal stresses (σ and $\bar{\sigma}$) are positive in compression. The friction at the slip surface follows a slip-weakening description and drops from static f_s to dynamic f_d linearly over a characteristic slip D_c: $f_{sw}=f_s-(f_s-f_d)min\{\delta,D_c\}/D_c$. In addition to the depth of the slip surface H, the friction law sets a second model length scale proportional to $GD_c/\bar{\sigma}_o(f_s-f_d)\equiv\tilde{R}$. Rupture is nucleated by the Andrews (1985) forced expansion of slip as described by Dunham and Rice (2008), $f_e(x,t)=max\left\{f_d+A\left(|x|-v_e t\right),f_d\right\}$ where $A=(f_s-f_d)/\tilde{R}$ and $v_e=0.144c_s$. The imposed friction coefficient is $f=\min\left\{f_{sw},f_e\right\}$ such that the friction coefficient is determined by f_{sw} beyond nucleation. Furthermore, the slip-surface

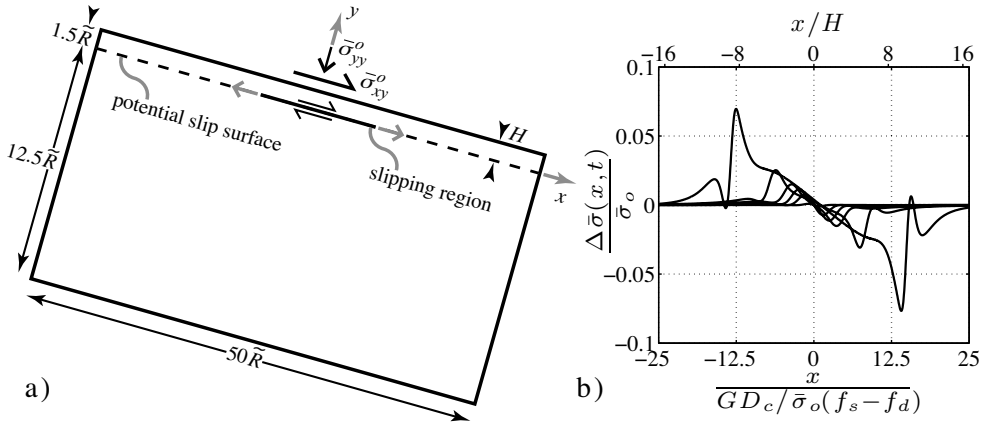

Figure 3: a) Schematic of portion of model domain (actual downdip length $100\tilde{R}$), initial stresses, and subsequent behavior. b) Snapshots of effective normal stress along the slip surface at intervals of $3.75\ \tilde{R}/c_s$ for a subsurface rupture at a depth $H = 1.5\tilde{R}$ in a saturated poroelastic body. Rupture shows preferred downslope propagation and significant normal stress changes. Model initial stress state is defined as $\bar{\sigma}^o_{yy} = (\gamma_b - \gamma_w)H\cos\theta$, $\bar{\sigma}^o_{xy} = (\gamma_b - \gamma_w)H\sin\theta$, $\bar{\sigma}^o_{xx} = K_o\bar{\sigma}^o_{yy}$, and $\bar{\sigma}^o_{zz} = (\bar{\sigma}^o_{xx} + \bar{\sigma}^o_{yy})/2$, where $\gamma_b = 1.75\gamma_w$, $\theta = 15.75°$, and $K_o = 1$. Surface frictional parameters are $f_p = 0.45$, $f_r = 0.2$, and $t^* = 0.015\tilde{R}/c_s$. Bulk poroelastic parameters are $G = 600\bar{\sigma}^o_{yy}$, $\nu = 0.35$, $\nu_u = 0.483$, and $B = 0.94$.

strength is time-regularized to follow $d\tau/dt = -[\tau - f(\sigma - p)]/t^*$ where t^* is the associated timescale, here small in comparison to a physical slip-surface timescale $\tilde{R}/c_s$.

The initial state of stress is uniform, consistent with the components of stress of a material element in a submerged infinite slope at a depth H (consistent shear and normal tractions are applied at the surface to maintain the initial state). A nonuniform stress state of depth-dependent stresses would not affect slope-parallel rupture if the surroundings deform elastically. The material away from the slip surface may deform elastically or elastic-plastically. The material yield strength model is based on a heavily overconsolidated clay assuming changes of stress occur in the dilative region of the yield surface where strength is approximated by a linear dependence on effective pressure (i.e., constant μ) and neglecting drained cohesion (i.e., $b = 0$). Under dynamic rupture the rapid deformation leaves little time for fluid flux and undrained conditions are assumed away from the surface. To calculate the pore pressure change on the surface, in the elastic regime we use (X.12), and during elastic-plastic deformation (localized at the rupture tip), we approximate the surface pressure with a similar weighting, replacing β^{el}_{stor} with β^{pl}_{stor} given at the onset of yielding and neglect changes in permeability. We calculate the undrained pore pressure increment used in that expression as that resulting from (X.10) with $dm = 0$. Near surface (disturbed region) material parameters are consistent with far-field parameters, except for a twofold reduction of the shear modulus near the slip surface. Model poroelastic parameters and stress state are summarized in the caption of Figure 3.

The effects of the slope surface on the slip surface become significant when the lengths become comparable. For $H/\tilde{R} \to \infty$ the solution approaches that of a crack in an unbounded medium under uniform initial loading, the case typically considered in earthquake source physics. In that limit, there is no effective normal stress change and no preferred rupture direction for a poroelastic medium when there is no contrast in material properties across the surface. For the poroelastic case when H and $\tilde{R}$ are comparable, total normal stress changes on the fault induce corresponding pore pressure changes and the

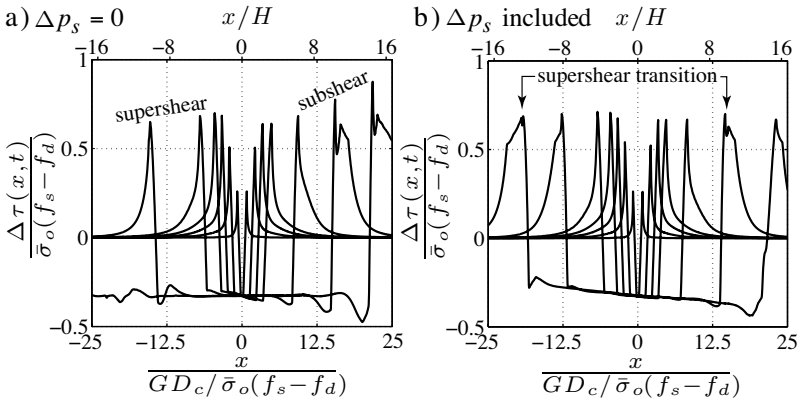

Figure 4: Snapshots of slip surface shear stress changes in elastic-plastic saturated medium a) neglecting slip surface pore pressure changes and b) including elastic-plastic effects on pore pressure changes.

net effective stress change induces a downslope preference for rupture (Figure 3b). Here, rupture propagation is below the Rayleigh wave speed c_r (for $\nu_u = 0.483$, $c_r \approx 0.95 c_s$) until about the last time step plotted in Figure 3b where the rupture begins a transition to rupture propagation beyond the shear wave speed (so-called supershear rupture), first in the downslope direction and shortly followed by a transition in the upslope direction (not shown). These transitions are remarkable since in an unbounded elastic medium this would normally occur for initial slip-surface shear stress states satisfying $r = (\bar{\sigma}^o_{xy} / \bar{\sigma}^o_{yy} - f_r)/(f_p - f_r) \gtrsim 0.36$ (Andrews 1976) and here $r = 0.32$ (note $r = 1/(1+S)$ where S is a similar measure commonly used in earthquake rupture studies).

With the introduction of plasticity, we find the preference for downslope rupture propagation is enhanced when pressure changes at the slip surface are included compared to when they are not. For initial simplicity, we maintain the conditions as in Figure 3 and take $\mu = 0.42$, $\beta = 0.3$, and $b = 0$. Neglecting surface pore pressure changes (Figure 4a) results in a preference to upslope rupture, which reaches supershear propagation speeds first, while the downslope rupture continues at subshear speeds. In the case considering surface pore pressure change (Figure 4b) there is longer delay to the supershear transition and a slight downslope preference with an initial transition to supershear occurring in the downslope direction, followed shortly by an upslope transition.

4. Conclusions

We considered a slip surface within a saturated, porous elastic-plastic medium and derived an approximate equation governing the pore pressure around that surface. That equation takes the form of a diffusion equation with a plastic hydraulic diffusivity, which, in addition to an evolving permeability, also includes a plastic storage coefficient. The storage coefficient may be several times larger than the original elastic storage, which decreases the diffusivity for fixed permeability. We applied this consideration to the dynamic propagation of a slope-parallel subsurface shear rupture. We found that considerable surface effects, most notably normal stress changes, provide a downslope directionality.

Acknowledgments This study was supported by NSF-EAR grants 0510193 and 0809610 and by an IODP Schlanger Fellowship to Robert Viesca. We thank Eric Dunham for helpful discussion and Ronaldo I. Borja and René de Borst for their reviews.

References

Andrews DJ (1976) Rupture velocity of plane strain shear cracks. J Geophys Res 81: 5679–5687

Andrews DJ (1985) Dynamic plane-strain shear rupture with a slip-weakening friction law calculated by a boundary integral method. Bull Seismol Soc Am 75(1): 1–21

Bishop AW (1971) The influence of progressive failure on the choice of the method of stability analysis. Géotechnique 21: 168–172

Bizzarri A, Cocco M (2006) A thermal pressurization model for the spontaneous dynamic rupture propagation on a three-dimensional fault: 1. Methodological approach. J Geophys Res 111(B05303), doi:10.1029/2005JB003862

de Borst R, Réthoré J, Abellan M-A (2006) A numerical approach for arbitrary cracks in a fluid-saturated medium. Arch Appl Mech 75: 595–606, doi: 10.1007/s00419-006-0023-y

Bjerrum L (1967) Progressive failure in slopes of overconsolidated plastic clay and clay shales. Trans Am Soc Civ Eng SM 93: 3–49

Cooper MR, Bromhead EN, Petley DJ, Grant DI (1998) The Selbourne cutting stability experiment. Géotechnique 48(1): 83–101

Dugan B, Flemings PB (2000) Overpressure and fluid flow in the New Jersey continental slope: implications for slope failure and cold seeps. Science 289: 288–291, doi:10.1126/science.289.5477.288

Dunham EM, Rice JR (2008) Earthquake slip between dissimilar poroelastic materials. J. Geophys. Res. 113(B09304), doi:10.1029/2007JB005405

Iverson RM, Reid ME, Iverson NR, LaHusen RG, Logan M, Mann JE, Brien DL (2000) Acute sensitivity of landslide rates to initial soil porosity. Science 290: 513–516

Lambe TW, Whitman RV (1969) Soil mechanics. John Wiley and Sons, New York

Mitchell TM, Faulkner DR (2008) Experimental measurements of permeability evolution during triaxial compression of initially intact crystalline rocks and implications for fluid flow in fault zones. J Geophys Res 113(B11412), doi:10.1029/2008JB005588

Moore PL, Iverson NR (2002) Slow episodic shear of granular materials regulated by dilatant strengthening. Geology 30(9): 843–846, doi:10.1130/0091-7613(2002)030<0843:SESOGM>2.0.CO;2

Palmer AC, Rice JR (1973) The growth of slip surfaces in the progressive failure of over-consolidated clay. Proc Roy Soc Lond A 332: 527–548

Puzrin AM, Germanovich LN (2005) The growth of shear bands in the catastrophic failure of soils. Proc Roy Soc A 481: 1199–1228 doi:10.1098/rspa.2004.1378

Puzrin AM, Germanovich LN, Kim S (2004) Catastrophic failure of submerged slopes in normally consolidated sediments. Géotechnique 54(10): 631–643

Réthoré J, de Borst R, Abellan M-A (2007) A discrete model for the dynamic propagation of shear bands in a fluid-saturated medium. Int J Numer Anal Meth Geomech 31: 347–370, doi: 10.1002/nag.575

Rice JR (1980) The mechanics of earthquake rupture. In: Dziewonski AM, Boschi E (eds) Physics of the Earth's interior (Proc International School of Physics 'Enrico Fermi', Course 78, 1979), Italian Phys Soc and North-Holland Publ Co: 555–639

Rice JR, Cleary MP (1976) Some basic stress diffusion solutions for fluid-saturated elastic porous media with compressible constituents. Rev. Geophys. Space Phys. 14(2): 227–241

Rudnicki JW (2001) Diffusive instabilities in dilating and compacting geomaterials. In: Chuang TJ, Rudnicki JW (eds) Multiscale deformation and fracture in materials and structures, Kluwer Acad., New York

Rudnicki JW, Rice JR (1975) Conditions for the localization of deformation in pressure-sensitive dilatant materials. J. Mech. Phys. Solids 23:371–394

Rudnicki JW, Rice JR (2006) Effective normal stress alteration due to pore pressure changes induced by dynamic slip propagation on a plane between dissimilar materials. J Geophys Res 111(B09314), doi:10.1029/2006JB004314

Segall P, Rice JR (1995) Dilatancy, compaction, and slip instability of a fluid-infiltrated fault. J Geophys Res 100(B11): 22,155–22171

Suzuki T and Yamashita T (2008) Nonlinear effects of temperature, fluid pressure, and inelastic porosity on dynamic fault slip and fault tip propagation: emergence of slip strengthening and pulse-like fault slip. J Geophys Res 113(B07304), doi:101.1029/2008JB005581

Templeton EL, Rice JR (2008) Off-fault plasticity and earthquake rupture dynamics: 1. Dry materials or neglect of fluid pressure changes. J Geophys Res 113(B09306) doi:10.1029/2007JB005529

Xu W, Germanovich LN (2006) Excess pore pressure resulting from methane hydrate dissociation in marine sediments: a theoretical approach. J Geophys Res 111(B01104), doi:10.1029/2004JB003600

Viesca RC, Templeton EL, Rice JR (2008) Off-fault plasticity and earthquake rupture dynamics: 2. Effects of fluid saturation. J Geophys Res 113(B09307) doi:10.1029/2007JB005530

White JA, Borja RI (2008) Stabilized low-order finite elements for coupled solid-deformation/fluid-diffusion and their application to fault zone transients. Comput Methods Appl Mech Eng 197, 4353–4366, doi: doi:10.1016/j.cma.2008.05.015